

# Vector level identity for dynamic subgrid scale modeling in large eddy simulation

Youhei Morinishi<sup>a)</sup>

Department of Mechanical Engineering, Nagoya Institute of Technology, Gokiso-cho, Showa-ku, Nagoya 466-8555, Japan

Oleg V. Vasilyev

Department of Mechanical Engineering, University of Colorado at Boulder, 427 UCB, Boulder, Colorado 80309-0427

(Received 9 January 2002; accepted 12 June 2002; published 5 September 2002)

The most commonly used dynamic subgrid scale model is based on the Smagorinsky eddy viscosity model with the model coefficient computed dynamically through the *tensor level* identity by Germano *et al.* However, the tensor level identity does not explicitly account for the effect of the discretization of the governing equations, and thus the computational results strongly depend on grid resolution, especially in a simulation with poor resolution. In this paper, we propose a new dynamic procedure with the *vector level* identity, which takes the effect of grid resolution into consideration. The new procedure is tested for the dynamic Smagorinsky eddy viscosity model with the vector level identity. All computational tests were done on turbulent channel flow. The numerical results confirm that the mean velocity profile computed using the new subgrid scale model does not depend on the grid resolution. © 2002 American Institute of Physics. [DOI: 10.1063/1.1504450]

## I. INTRODUCTION

The objective of this study is to develop a dynamic subgrid scale model for large eddy simulation of turbulent flows, for which computational results are independent of grid resolution. The most commonly used dynamic subgrid scale model is based on the Smagorinsky eddy viscosity model<sup>1</sup> with the model coefficient computed dynamically through the *tensor level* identity by Germano *et al.*<sup>2</sup> However, the tensor level identity does not explicitly account for the effect of the discretization of the equations governing the evolution of the large-scale turbulent velocity field, and thus the computational results strongly depend on grid resolution, especially in simulations with poor resolution. In this paper we will present a new dynamic procedure with the *vector level* identity, which takes the discretization effect into consideration. The original idea was first introduced by Morinishi and Vasilyev,<sup>3</sup> and in this paper we present a more detailed analysis. This new dynamic procedure is tested for the Smagorinsky eddy viscosity model with the vector level identity. Computational tests are done on turbulent channel flow with Reynolds numbers based on the channel half-width and wall friction velocity of 180, 395, and 590.

The present paper is organized as follows. In Sec. II the dynamic procedure for subgrid scale modeling with the vector level identity is proposed. The standard dynamic procedure with the tensor level identity (Germano identity) is also introduced for a comparison. In Sec. III the large eddy simulations of plane channel flow are performed and the compu-

tational results are compared with those of the standard dynamic Smagorinsky model. The effects of grid resolution and the Reynolds number on the computational results are discussed. Section IV contains conclusions of this study.

## II. TENSOR AND VECTOR LEVEL IDENTITIES FOR THE DYNAMIC SUBGRID SCALE MODELING

### A. Filtered Navier–Stokes and continuity equations

The governing equations for incompressible flows are the Navier–Stokes and continuity equations, given by

$$\frac{\partial u_i}{\partial t} + \frac{\partial u_i u_j}{\partial x_j} = -\frac{\partial p}{\partial x_i} + \nu \frac{\partial^2 u_i}{\partial x_j \partial x_j}, \quad (1)$$

$$\frac{\partial u_i}{\partial x_i} = 0. \quad (2)$$

Here  $u_i$  is the velocity component in the  $x_i$  direction ( $i = 1, 2, 3$ ),  $p$  is the pressure divided by the density,  $\nu$  is the kinematic viscosity, and  $t$  is time.

In large eddy simulation with dynamic subgrid scale modeling, two different filters, i.e., the grid filter  $\bar{G}(\mathbf{x})$  and the test filter  $\hat{G}(\mathbf{x})$ , are introduced:

$$\bar{\phi}(\mathbf{x}, t) = \int \bar{G}(\mathbf{x} - \mathbf{x}') \phi(\mathbf{x}', t) d^3 \mathbf{x}', \quad (3)$$

$$\hat{\phi}(\mathbf{x}, t) = \int \hat{G}(\mathbf{x} - \mathbf{x}') \phi(\mathbf{x}', t) d^3 \mathbf{x}'. \quad (4)$$

Applying the grid filter (3) to Eqs. (1) and (2), we get the following governing equations for the grid filtered flow field  $(\bar{u}_i, \bar{p})$ :

<sup>a)</sup> Author to whom correspondence should be addressed. Telephone: +81 52 735 5346; fax: +81 52 735 5342; electronic mail: morinishi@efd.mech.nitech.ac.jp

$$\frac{\partial \bar{u}_i}{\partial t} + \frac{\overline{\partial u_i u_j}}{\partial x_j} = -\frac{\partial \bar{p}}{\partial x_i} + \nu \frac{\partial^2 \bar{u}_i}{\partial x_j \partial x_j}, \quad (5)$$

$$\frac{\partial \bar{u}_i}{\partial x_i} = 0. \quad (6)$$

The commutability between the differentiation and filtering operations is usually assumed and the filtered convection term is treated as

$$\frac{\overline{\partial u_i u_j}}{\partial x_j} = \frac{\partial \bar{u}_i \bar{u}_j}{\partial x_j} + \frac{\partial \tau_{ij}}{\partial x_j}, \quad (7)$$

$$\tau_{ij} = \overline{u_i u_j} - \bar{u}_i \bar{u}_j, \quad (8)$$

where  $\tau_{ij}$  is the subgrid scale stress which should be modeled.

In large eddy simulation with the dynamic subgrid scale model, the governing equations for the test filtered flow field ( $\hat{u}_i, \hat{p}$ ) are obtained by applying the test filter (4) to Eqs. (5) and (6):

$$\frac{\partial \hat{u}_i}{\partial t} + \frac{\widehat{\partial u_i u_j}}{\partial x_j} = -\frac{\partial \hat{p}}{\partial x_i} + \nu \frac{\partial^2 \hat{u}_i}{\partial x_j \partial x_j}, \quad (9)$$

$$\frac{\partial \hat{u}_i}{\partial x_i} = 0. \quad (10)$$

The commutability is assumed once again and the filtered convection term is given by

$$\frac{\widehat{\partial u_i u_j}}{\partial x_j} = \frac{\partial \hat{u}_i \hat{u}_j}{\partial x_j} + \frac{\partial T_{ij}}{\partial x_j}, \quad (11)$$

$$T_{ij} = \widehat{u_i u_j} - \hat{u}_i \hat{u}_j, \quad (12)$$

where  $T_{ij}$  is called the subtest scale stress.

## B. Dynamic subgrid scale modeling with tensor level identity (standard dynamic modeling)

In the standard dynamic subgrid scale modeling, the tensor level identity of Germano *et al.*<sup>2</sup> between the subgrid and subtest scale stresses is used to determine the parameter in the subgrid scale model,

$$\mathcal{L}_{ij} = T_{ij} - \hat{\tau}_{ij}, \quad (13)$$

where the resolved stress  $\mathcal{L}_{ij}$  is defined as

$$\mathcal{L}_{ij} = \widehat{u_i u_j} - \hat{u}_i \hat{u}_j. \quad (14)$$

In the standard dynamic SGS model the Smagorinsky eddy viscosity model is assumed for both the subgrid and subtest scale stresses:

$$\tau_{ij}^* = -2(C_S \bar{\Delta})^2 |\bar{S}| \bar{S}_{ij}, \quad \bar{S}_{ij} = \frac{1}{2} \left( \frac{\partial \bar{u}_i}{\partial x_j} + \frac{\partial \bar{u}_j}{\partial x_i} \right),$$

$$|\bar{S}| = (2\bar{S}_{ij}\bar{S}_{ij})^{1/2}, \quad (15)$$

$$T_{ij}^* = -2(C_S \hat{\Delta})^2 |\hat{S}| \hat{S}_{ij}, \quad \hat{S}_{ij} = \frac{1}{2} \left( \frac{\partial \hat{u}_i}{\partial x_j} + \frac{\partial \hat{u}_j}{\partial x_i} \right),$$

$$|\hat{S}| = (2\hat{S}_{ij}\hat{S}_{ij})^{1/2}. \quad (16)$$

The superscript “\*” denotes the trace-free operator ( $\tau_{ij}^* \equiv \tau_{ij} - \frac{1}{3}\delta_{ij}\tau_{kk}$ ). Following Lilly,<sup>4</sup> the model parameter  $C_S$  is computed by minimizing the square of the error  $Q^T = E_{ij}E_{ij}$ :

$$E_{ij} = \mathcal{L}_{ij}^* + 2(C_S \bar{\Delta})^2 M_{ij}, \quad M_{ij} = \alpha^2 |\hat{S}| \hat{S}_{ij} - |\bar{S}| \bar{S}_{ij}. \quad (17)$$

Here  $\alpha^2 = (\hat{\Delta}/\bar{\Delta})^2$  is the square value of the test to grid filter widths ratio. In this study we take  $\alpha^2 = 5^{2/3} \sim 2.92$ . It corresponds to<sup>5</sup>  $\hat{\Delta}_1 = \sqrt{5}\bar{\Delta}_1$ ,  $\hat{\Delta}_2 = \bar{\Delta}_2$ , and  $\hat{\Delta}_3 = \sqrt{5}\bar{\Delta}_3$ . Assuming  $C_S$  is a function of  $x_2$  and taking the average in the  $x_1-x_3$  plane (denoted by  $\langle \cdot \rangle$ ), we obtain the following equation for  $(C_S \bar{\Delta})^2$ :

$$(C_S \bar{\Delta})^2 = -\frac{1 \langle \mathcal{L}_{ij} M_{ij} \rangle}{2 \langle M_{ij} M_{ij} \rangle}. \quad (18)$$

In this paper the dynamic Smagorinsky model given by Eqs. (15) and (18) is called DSM.

## C. Dynamic subgrid scale modeling with vector level identity

In practical LES applications the finite difference method is usually used and the first term on the right-hand side of Eq. (7) is approximated by

$$\frac{\delta \bar{u}_i \bar{u}_j}{\delta x_j} \sim \frac{\partial \bar{u}_i \bar{u}_j}{\partial x_j} + O(h^n),$$

where  $\delta u_i u_j / \delta x_j$  denotes the  $n$ th-order accurate finite difference approximation to  $\partial u_i u_j / \partial x_j$  and  $O(h^n)$  is the truncation error. This means that the filtered convection term, Eq. (7), suffers from the discretization effect, even if we know the exact subgrid stress. That is why the development of high-order numerical methods has been considered as one of the important areas of LES research.<sup>6</sup>

In this study, we propose an alternative approach to improve the reliability of the computational results of LES. The filtered convection term in the grid field is modeled as

$$\frac{\overline{\partial u_i u_j}}{\partial x_j} = \frac{\delta \bar{u}_i \bar{u}_j}{\delta x_j} + \frac{\partial \tau_{ij}}{\partial x_j}, \quad (19)$$

where the numerical error is treated as a part of the subgrid scale stress (exactly, subgrid scale vector), and the rest is modeled with  $\tau_{ij}$ . The filtered convective term in the test field is assumed as follows:

$$\frac{\widehat{\partial u_i u_j}}{\partial x_j} = \frac{\delta \hat{u}_i \hat{u}_j}{\delta x_j} + \frac{\partial T_{ij}}{\partial x_j}. \quad (20)$$

The model parameter in the dynamic subgrid scale model is determined through the following vector level identity:

$$C_i = \frac{\partial T_{ij}}{\partial x_j} - \frac{\widehat{\partial \tau_{ij}}}{\partial x_j}, \quad (21)$$

where the resolved convection term,  $C_i$ , is defined as

$$C_i = C_{ij}^i, \quad C_{ij}^k = \frac{\widehat{\delta \bar{u}_i \bar{u}_j}}{\delta x_k} - \frac{\delta \hat{u}_i \hat{u}_j}{\delta x_k}. \quad (22)$$

If the parameter in the dynamic subgrid scale model is estimated through the vector level identity given by Eq. (21), then the discretization effect on the convection term explicitly influences the model parameter. Substituting Eqs. (15) and (16) into Eq. (21), we obtain the following error  $E_i$  and its square value:

$$Q^V = E_i E_i, \quad E_i = C_i^* + 2M_i (C_S \bar{\Delta})^2 + 2M_{ij} \frac{\partial (C_S \bar{\Delta})^2}{\partial x_j}, \quad (23)$$

where

$$C_i^* = C_i - \frac{1}{3} \delta_{ij} C_{kk}^i, \quad M_i = \frac{\partial M_{ij}}{\partial x_j}.$$

Note that in contrast to the tensor level identity, the error term  $Q^V$  depends not only on the values of  $(C_S \bar{\Delta})^2$  but also on its derivatives. As a consequence, the minimization procedure is no longer local and we need to use the variational principal to determine  $(C_S \bar{\Delta})^2$ . In this study,  $(C_S \bar{\Delta})^2$  is estimated by minimizing the following weighted integral:

$$\int \int \int w(x_2) Q^V(x_1, x_2, x_3) dx_1 dx_2 dx_3. \quad (24)$$

Following the general variational principle it can be shown that if the function  $\phi(y)$  provides the minimum for the weighted integral,

$$\int w(y) \left( A + B \cdot \phi + C \frac{d\phi}{dy} \right)^2 dy,$$

then it should also satisfy the following differential equation:

$$w(y) \left( A + B \cdot \phi + C \frac{d\phi}{dy} \right) B - \frac{d}{dy} \left[ w(y) \left( A + B \cdot \phi + C \frac{d\phi}{dy} \right) C \right] = 0.$$

Assuming that  $C_S$  is a function of  $x_2$  and taking the average in the periodic directions, the  $(C_S \bar{\Delta})^2$  value, which minimizes the weighted integral (24), is obtained through the variational principal, which leads to the following differential equation:

$$w(x_2) \left[ \langle M_i M_i \rangle (C_S \bar{\Delta})^2 + \langle M_{i2} M_i \rangle \frac{d(C_S \bar{\Delta})^2}{dx_2} \right] - \frac{d}{dx_2} \left[ w(x_2) \left( \langle M_i M_{i2} \rangle (C_S \bar{\Delta})^2 + \langle M_{i2} M_{i2} \rangle \frac{d(C_S \bar{\Delta})^2}{dx_2} \right) \right] = R(x_2), \quad (25)$$

where

$$R(x_2) = -\frac{1}{2} w(x_2) \langle C_i^* M_i \rangle + \frac{1}{2} \frac{d[w(x_2) \langle C_i^* M_{i2} \rangle]}{dx_2}.$$

Equation (25) is discretized using the second-order finite difference method and is solved using the direct tridiagonal solver. In this study the weight is selected as  $w(x_2) = 1/h_2(x_2)$ , where  $h_2(x_2)$  is the grid spacing in  $x_2$ . As will

be shown in Sec. III A, the value of  $(C_S \bar{\Delta})^2$  determined by Eq. (25) can become negative very close to the wall. Negative values of  $(C_S \bar{\Delta})^2$  can lead to numerical instabilities. One way to deal with this issue is to introduce simple negative clipping, which will result in a discontinuous  $C_S$  profile. An alternative procedure to deal with this issue will be discussed in Sec. III A. For the clarity of discussion, the dynamic Smagorinsky model given by Eq. (15) with  $(C_S \bar{\Delta})^2$  determined by Eq. (25) will be referred to as VDSMwmc, where the last two letters stand for ‘‘without clipping.’’

Note that the dynamic procedure assumes the model similarity for both grid and test filters (see Meneveau and Katz<sup>8</sup>). However, the test filter size is bigger. Thus, in order to achieve complete model similarity at test and grid levels, the truncation error should be proportionally greater. This can only be achieved for the second-order method, and will never be true for higher-order schemes. However, for higher-order schemes and filters with a nonvanishing second moment the truncation error is considerably lower than commutation error. Thus, complete proportionality of the truncation error is not crucial. We also note that the subgrid scale model with the vector level identity does not assume the commutability between the differentiation and filtering operation:

$$\overline{\frac{\partial u_i u_j}{\partial x_j}} \neq \frac{\partial \overline{u_i u_j}}{\partial x_j}.$$

### III. LES RESULTS AND DISCUSSION

In this study the numerical tests for subgrid scale models with both the tensor and vector level identities are performed using fully developed plane channel flow at a Reynolds number of 180, 395, and 590. The flow field is assumed to be periodic in the streamwise ( $x_1$ ) and spanwise ( $x_3$ ) directions. The Reynolds number ( $Re_\tau = u_\tau H/\nu$ ) is based on the channel half-width  $H$  and the wall friction velocity  $u_\tau$ . The filtering operations in the dynamic subgrid scale models are performed only in the periodic directions. The test filtering with the filter width  $\hat{\Delta}_i = 2h_i$  in  $x_i$ ,  $i=1,3$ , directions is done as follows:

$$\hat{f}(x_i) = \frac{1}{6} [f(x_i - h_i) + 4f(x_i) + f(x_i + h_i)]. \quad (26)$$

Table I summarizes the grid resolution for all computational cases in this study. The computational box for all cases is  $2\pi H \times 2H \times 2\pi H/3$ . Cases B–F correspond to the flow at  $Re_\tau = 395$  and different grid resolutions in the periodic directions. Case A corresponds to the flow at lower Reynolds number  $Re_\tau = 180$ . Case G corresponds to the flow at higher Reynolds number  $Re_\tau = 590$ . The grid spacings in the periodic directions are uniform. The wall normal grid is stretched using a hyperbolic-tangent function. The mixed order fully conservative finite difference scheme in a staggered grid system is used, where the fourth-order accurate discretization proposed by Morinishi *et al.*<sup>7</sup> is used in homogeneous directions and the second-order one is used in the wall normal direction. The computational method is the same as that in Morinishi and Vasilyev.<sup>9</sup> In this study we shall compare the dynamic vector model with the dynamic tensor one with re-

TABLE I. Computational cases.

Case	$Re_\tau$	$L_1$	$L_2$	$L_3$	$N_1$	$N_2$	$N_3$	$h_1^+$	$h_2^+$	$h_3^+$
Case A	180	$2\pi H$	$2H$	$2\pi H/3$	32	64	32	35.3	0.6–12.9	11.8
Case B	395	$2\pi H$	$2H$	$2\pi H/3$	16	64	16	155.1	0.6–34.1	51.7
Case C	395	$2\pi H$	$2H$	$2\pi H/3$	24	64	24	103.4	0.6–34.1	34.5
Case D	395	$2\pi H$	$2H$	$2\pi H/3$	32	64	32	77.6	0.6–34.1	25.9
Case E	395	$2\pi H$	$2H$	$2\pi H/3$	48	64	48	51.7	0.6–34.1	17.2
Case F	395	$2\pi H$	$2H$	$2\pi H/3$	64	64	64	38.8	0.6–34.1	12.9
Case G	590	$2\pi H$	$2H$	$2\pi H/3$	32	64	32	115.8	0.6–55.4	38.6

spect to the grid resolution only, since the dependence of the LES result on the order of accuracy and on grid resolution with some existing subgrid scale models has been discussed by Morinishi and Vasilyev.<sup>9</sup> The computational cases, cases C–F, correspond to cases 1–4 of Ref. 9.

### A. Model comparison for case D and negative clipping

Figure 1 shows the profiles of mean streamwise velocity  $U_1$  ( $U_1 = \langle \bar{u}_1 \rangle_t$ ) of the channel flow at  $Re_\tau = 395$  (case D) using VDSMwc, DSM, and No SGS. The ensemble averaging over the  $x_1 - x_3$  plane and time is denoted by  $\langle \cdot \rangle_t$ . In this paper, variables with superscript “+” are normalized by the wall friction velocity  $u_\tau$  and the viscous length scale  $\delta_v$  ( $\delta_v = \nu/u_\tau$ ). The simulations without a subgrid scale model are labeled as No SGS. In the figure the corresponding DNS data by Moser *et al.*<sup>10</sup> are also plotted. Note that for visual clarity only one-third of the DNS data points are plotted. The difference between the mean velocity profiles for No SGS and the DNS results should be properly compensated by a subgrid scale model, as discussed in Morinishi and Vasilyev.<sup>9</sup> The profile using VDSMwc coincides well with the DNS data, while the mean velocity with DSM is too large.

Figure 2 shows the profiles of the grid scale velocity fluctuations ( $u'_\alpha = \sqrt{\langle \bar{u}_\alpha^2 \rangle_t - \langle \bar{u}_\alpha \rangle_t^2}$ ,  $\alpha = 1, 2, 3$ ) and the grid scale Reynolds shear stress ( $u'_1 u'_2 = \langle \bar{u}_1 \bar{u}_2 \rangle_t - \langle \bar{u}_1 \rangle_t \langle \bar{u}_2 \rangle_t$ ) using VDSMwc, DSM, and No SGS. The peak value of the streamwise velocity fluctuation of the simulation without a subgrid scale model is higher than that of the DNS data. The defect is not cured in the results of VDSMwc and DSM. This defect is caused by the finite difference simulation and it is

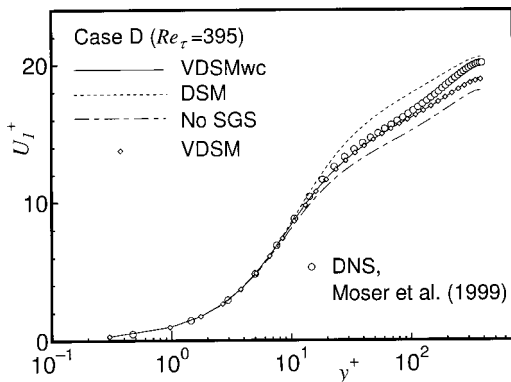


FIG. 1. The mean streamwise velocity profiles for the channel flow simulation at  $Re_\tau = 395$  (case D) using VDSMwc, DSM, No SGS, and VDSM.

not cured completely by the addition of the dynamic Smagorinsky model.<sup>9</sup> We believe that the addition of a scale similarity model<sup>11–16,9</sup> should improve the profile. However, we leave it for future investigation.

Figure 3 shows the profiles of the parameter  $C_S$  near the wall. The parameter  $C_S$  is plotted as  $\text{sign}[(C_S \bar{\Delta})^2] \sqrt{|(C_S \bar{\Delta})^2| / (h_1 h_2 h_3)^{2/3}}$ . The  $C_S$  value of VDSMwc is negative very close to the wall, even if we introduce the plane averaging as in Eq. (25). Basically we do not want  $C_S$  to be negative by reason of the numerical stability problem. However, the simple negative clipping causes a discontinuous  $C_S$  profile. To overcome this difficulty we modify the minimization procedure. In particular, we will minimize the following integral:

$$\iiint \{w(x_2) Q^V(x_1, x_2, x_3) - F(x_2) (C_S \bar{\Delta})^2\} dx_1 dx_2 dx_3, \quad (27)$$

where  $F(x_2)$  is a non-negative function to be determined later. The motivation for this procedure is based on the simple observation that for positive  $F(x_2)$  and negative values of  $(C_S \bar{\Delta})^2$  the addition of the extra term to Eq. (27) increases the value of the integral. Applying the variational principal to Eq. (27) we obtain the following differential equation for the function minimizing the integral:

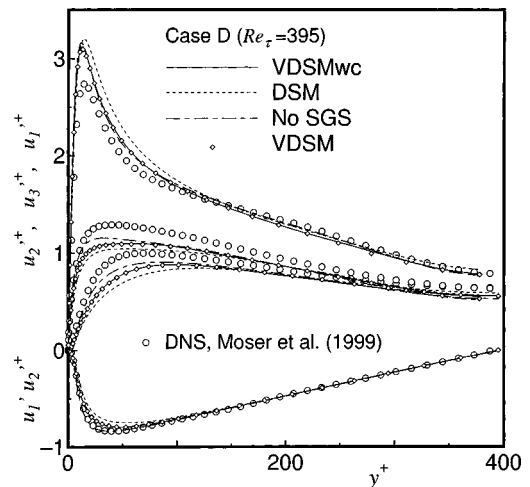


FIG. 2. The profiles of grid scale velocity fluctuations for the channel flow at  $Re_\tau = 395$  (case D) using VDSMwc, DSM, No SGS, and VDSM.

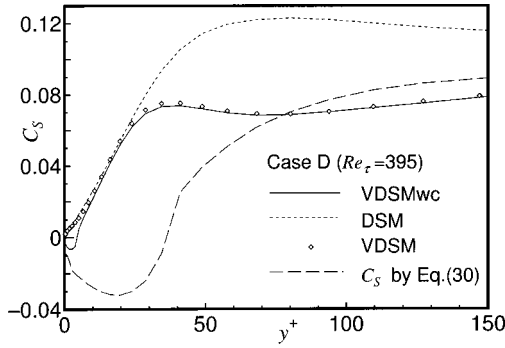


FIG. 3. The profiles of the model parameter  $C_s$  for the channel flow simulation at  $Re_\tau=395$  (case D) using VDSMwc, DSM, and VDSM. The  $C_s$  value computed by Eq. (30) is also plotted.

$$w(x_2) \left[ \langle M_i M_i \rangle (C_s \bar{\Delta})^2 + \langle M_{i2} M_i \rangle \frac{d(C_s \bar{\Delta})^2}{dx_2} \right] - \frac{d}{dx_2} \left[ w(x_2) \left( + \langle M_i M_{i2} \rangle (C_s \bar{\Delta})^2 + \langle M_{i2} M_{i2} \rangle \frac{d(C_s \bar{\Delta})^2}{dx_2} \right) \right] = R(x_2) + F(x_2). \quad (28)$$

The term  $\langle M_i M_i \rangle (C_s \bar{\Delta})^2$  is the most dominant term in Eq. (25), thus the negative values of  $(C_s \bar{\Delta})^2$  could occur when  $R(x_2)$  is negative. To eliminate this problem we set  $F(x_2)$  to be exactly zero where  $R(x_2)$  is positive and  $F(x_2) = -R(x_2)$  in the regions where  $R(x_2)$  is negative. This simple procedure is effectively equivalent to the clipping of the source term to Eq. (25) as

$$w(x_2) \left[ \langle M_i M_i \rangle (C_s \bar{\Delta})^2 + \langle M_{i2} M_i \rangle \frac{d(C_s \bar{\Delta})^2}{dx_2} \right] - \frac{d}{dx_2} \left[ w(x_2) \left( + \langle M_i M_{i2} \rangle (C_s \bar{\Delta})^2 + \langle M_{i2} M_{i2} \rangle \frac{d(C_s \bar{\Delta})^2}{dx_2} \right) \right] = \text{MAX}[R(x_2), 0], \quad (29)$$

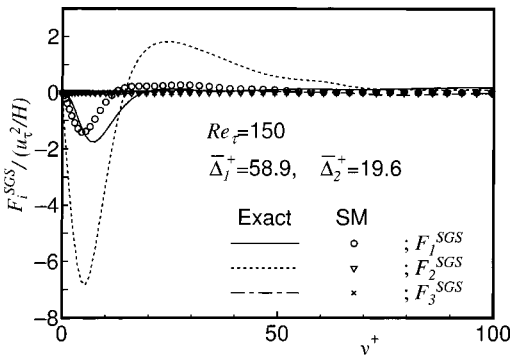


FIG. 4. The profiles of the exact SGS force and one modeled by SM. The data are extracted from a spectral DNS data of plane channel flow at  $Re_\tau=150$ .

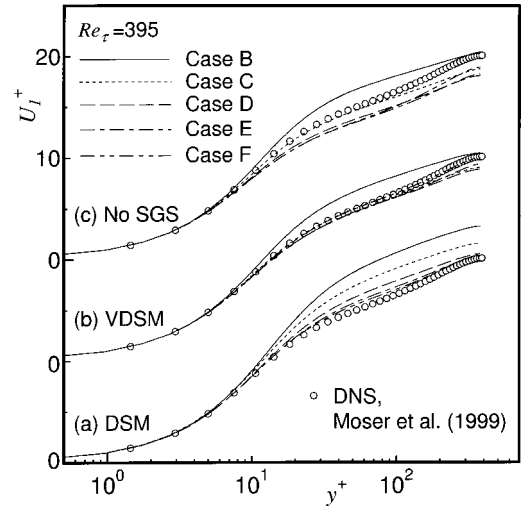


FIG. 5. The effect of grid resolution on the mean streamwise velocity profile for the channel flow at  $Re_\tau=395$  using DSM, VDSM, and No SGS.

where the function  $\text{MAX}[a, b]$  extracts the larger one. The small diamond ( $\diamond$ ) symbols in Figs. 1–3 are the results of VDSM with the clipping [using Eq. (29)]. The negative  $C_s$  value very close to the wall disappears and a smooth  $C_s$  profile is obtained by the source term clipping, as shown in Fig. 3. The effect of the clipping on the mean velocity and the fluctuation velocity profiles is negligible, as shown in Figs. 1 and 2. Hereafter, the dynamic Smagorinsky model given by Eq. (15) with  $(C_s \bar{\Delta})^2$  determined by Eq. (29) is called VDSM.

In order to understand the importance of the last term in Eq. (23), we consider a simplified dynamic procedure for the vector level identity proposed by Sagaut *et al.*<sup>17</sup> The simplification is achieved by removing the last term in Eq. (23) and applying the least square minimization:

$$(C_s \bar{\Delta})^2 = - \frac{1 \langle C_i^* M_i \rangle}{2 \langle M_i M_i \rangle}. \quad (30)$$

This simplified procedure was used in freely decaying turbulence and the results were better than that for the standard dynamic procedure.<sup>18</sup> The  $C_s$  value computed by Eq. (30) using the flow field of VDSMwc is also plotted in Fig. 3. The negative region of  $C_s$  given by Eq. (30) near the wall is wider, and the difference of the  $C_s$  value between Eqs. (25) and (30) is not negligible. This indicates the importance of the last term in Eq. (23) for wall bounded flows.

To clarify the reason why the negative  $C_s$  region appears very close to the wall for the eddy viscosity model with the vector level identity, a spectral DNS of the plane channel flow ( $Re_\tau: 150$ , box:  $4\pi H \times 2H \times 4\pi H/3$ , grid:  $128 \times 129 \times 128$ ) was performed and the exact SGS force,  $F_i^{SGS} = \langle \partial \tau_{i2}^* / \partial x_2 \rangle$ , was compared with the one modeled by the standard Smagorinsky model with the van Driest wall damping function with  $C_s=0.1$  (SM). Figure 4 shows the result of an *a priori* test for the SGS force. The grid scale velocity field is extracted from the DNS data using the plane filtering (Gaussian,  $\bar{\Delta}_1^+ = 58.9$ ,  $\bar{\Delta}_3^+ = 19.6$ ). A large difference between the exact and the modeled forces appears in the wall

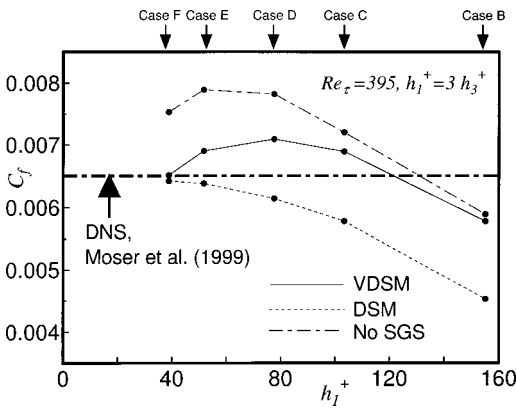


FIG. 6. The skin friction coefficient for the channel flow simulation at  $Re_\tau = 395$  using DSM, VDSM, and No SGS.

normal component close to the wall. This difference is caused by the isotropic representation of  $\tau_{ij}$ , while in reality  $\langle \tau_{22}^* \rangle \neq 0$ . Thus, the negative  $C_S$  value of VDSMwc close to the wall is the result of this defect.

**B. Dependence of the LES result on grid resolution**

Figure 5 shows the effect of the grid resolution on the profile of the mean streamwise velocity of the channel flow at  $Re_\tau = 395$  using VDSM, DSM, and No SGS. The grid resolutions corresponding to cases B–F are shown in Table I. With an increase in the grid resolution, the results of finite difference calculations converge. The numerical error of case B is considerably larger than those of the finer resolution cases (cases C–F). The mean velocity profiles of VDSM and DSM converge to the DNS data with an increase in grid resolution. However, DSM requires excessive grid resolution to reach the converged profile. On the other hand, the results of VDSM coincide well with the DNS data, except for a case with very poor grid resolution (case B).

Figure 6 shows the skin friction coefficient,  $C_f = 2\tau_w / (\rho U_m^2)$ , for the cases that appeared in Fig. 5, where  $\tau_w$

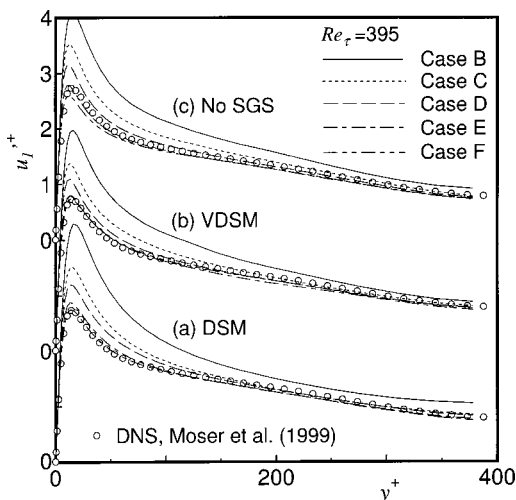


FIG. 7. The effect of grid resolution on the streamwise grid scale velocity fluctuation profile for the channel flow at  $Re_\tau = 395$  using DSM, VDSM, and No SGS.

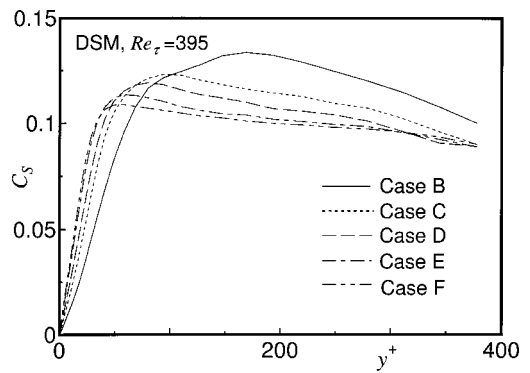


FIG. 8. The effect of grid resolution on  $C_S$  for the channel flow at  $Re_\tau = 395$  using DSM.

is the wall shear stress,  $\rho$  is the density, and  $U_m = 1/(2H) \int_{-H}^H U_1 dx_2$  is the bulk mean velocity. The  $C_f$  value of the DNS data by Moser *et al.*<sup>10</sup> is also plotted. The high intercept (constant  $B$ ) of the log law [ $U_1^+ = (1/\kappa) \ln y^+ + B$ ] for DSM is due to the low value of the skin friction coefficient, while the low intercept of the log law of No SGS for cases C–F is due to the high value of the skin friction coefficient. The VDSM model produces a reliable skin friction coefficient for a wide range of grid resolution. For case B, the  $C_f$  value of No SGS is lower than the DNS data. The addition of the Smagorinsky-type eddy viscosity model decreases the  $C_f$  value.<sup>9</sup> As a consequence, in order to get a reliable mean velocity profile, a grid resolution should be chosen so that the same resolution numerical simulation with no SGS model would result in a  $C_f$  that is higher than the DNS value. This is true, even for VDSM. Notice that this is the limitation of Smagorinsky-type models and is not of the vector level identity. The vector procedure with a different type of subgrid scale model would remove the limitation.

Figure 7 shows the effect of grid resolution on the profile of streamwise grid scale velocity fluctuation of the channel flow at  $Re_\tau = 395$  using VDSM, DSM, and No SGS. The peak value of the velocity fluctuation of VDSM, DSM, and No SGS for case B is much higher than the DNS data, and it improves by increasing the grid resolution. No apparent difference between the tensor and vector models is confirmed on the velocity fluctuation.

Figures 8 and 9 show the profiles of the parameter  $C_S$

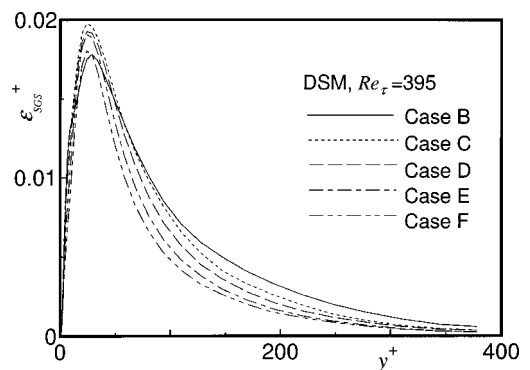


FIG. 9. The effect of grid resolution on the SGS dissipation of the GS turbulence energy for the channel flow at  $Re_\tau = 395$  using DSM.

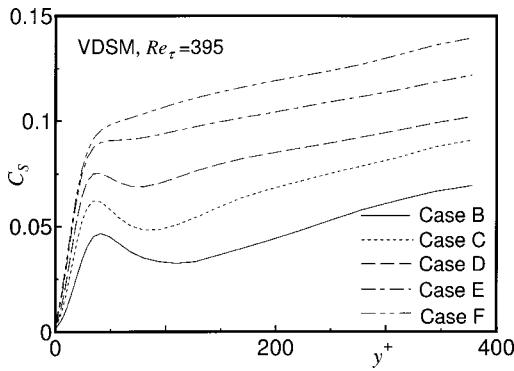


FIG. 10. The effect of grid resolution on  $C_s$  for the channel flow at  $Re_\tau = 395$  using VDSM.

and the SGS dissipation profiles using DSM. The SGS dissipation that appears in the transport equation of grid scale (GS) turbulence energy ( $k_{GS} = \frac{1}{2} \langle \bar{u}_i \bar{u}_i \rangle_t - \langle \bar{u}_i \rangle_t \langle \bar{u}_i \rangle_t$ ) is given by  $\epsilon_{SGS} = - \langle \tau_{ij} \bar{S}_{ij} \rangle_t + \langle \tau_{ij} \rangle_t \langle \bar{S}_{ij} \rangle_t$ . The peak value of  $C_s$  increases and its location moves away from the wall with decreasing the grid resolution as shown in Fig. 8. This produces an excessive SGS dissipation for the cases with poor grid resolution, as shown in Fig. 9, and results in the higher mean velocity (Fig. 5).

Figures 10 and 11 show the profiles of the parameter  $C_s$  and the SGS dissipation profiles using VDSM. The  $C_s$  and the dissipation values of VDSM decrease with decreasing the grid resolution. This behavior is expected and match well the mean velocity prediction, since the finite difference simulation with lower grid resolution requires lower subgrid scale contribution, as shown in Fig. 5(c). This indicates that the proposed procedure gives the proper model parameter that corresponds to the grid resolution.

**C. Dependence of the LES result on Reynolds number**

To confirm the dependence of the LES results on Reynolds number, further LES simulations are performed at three Reynolds numbers  $Re_\tau = 180, 395,$  and  $590$  that correspond to cases A, D, and G, respectively. The three cases have the same box size and grid number, as shown in Table I. Therefore the difference of the Reynolds number corre-

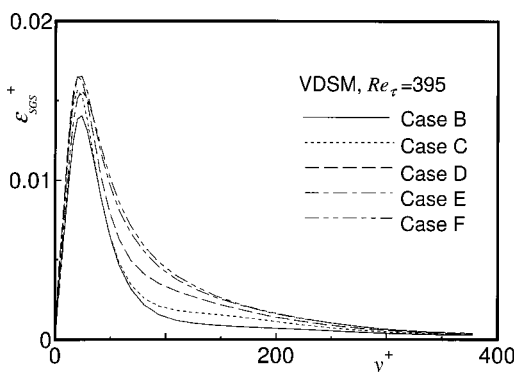


FIG. 11. The effect of grid resolution on the SGS dissipation of the GS turbulence energy for the channel flow at  $Re_\tau = 395$  using VDSM.

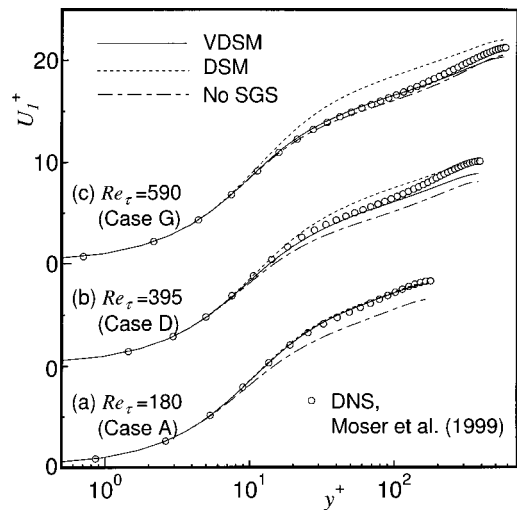


FIG. 12. The effect of Reynolds number on the mean streamwise velocity profile for the channel flow using VDSM, DSM, and No SGS.

sponds to the difference of the grid resolution in wall units. That is, the grid resolution of case A is relatively high while that of case G is relatively low.

Figures 12 and 13, respectively, show the effect of the Reynolds number on the profiles of mean streamwise velocity  $U_1$  and streamwise grid scale velocity fluctuation  $u'_1$  of the channel flow using VDSM, DSM, and No SGS. In these figures the DNS data of the corresponding Reynolds numbers by Moser *et al.*<sup>10</sup> are also plotted. The mean velocity profile with No SGS is lower for cases A and D, and slightly lower for case G than the corresponding DNS data. The profile with DSM is higher than the corresponding DNS data except for case A for which relatively high grid resolution is used. The VDSM model compensates the difference between the No SGS and DNS data properly for all the Reynolds number cases. The peak value of the streamwise velocity fluctuation increases with an increase of the Reynolds number, and no apparent difference between the models is con-

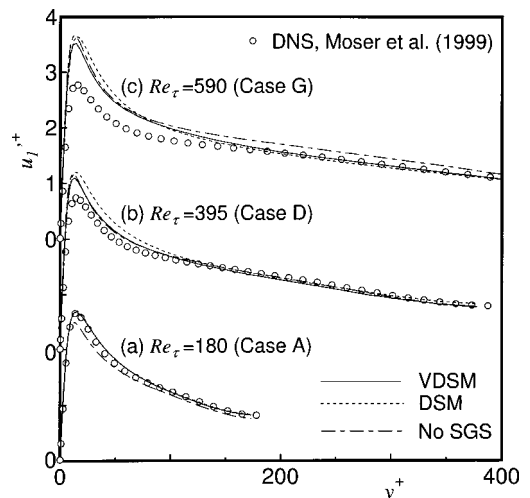


FIG. 13. The effect of Reynolds number on the streamwise grid scale velocity fluctuation profile for the channel flow using VDSM, DSM, and No SGS.

firmed. This trend simply reflects the dependence of the fluctuation profile on the grid resolution for a Smagorinsky-type subgrid scale model.

#### IV. CONCLUSIONS

A new dynamic procedure with the vector level identity for subgrid scale modeling was proposed and tested for the Smagorinsky eddy viscosity model. The differential equation for the model coefficient for the vector model is obtained using the variational principal. To avoid negative values for the model coefficient, the source term clipping procedure is introduced. All computational tests were done on turbulent channel flow, and the Reynolds numbers based on the channel half-width and wall friction velocity are 180, 395, and 590. Results of numerical simulations confirm that the mean velocity profile computed using the new dynamic subgrid scale model is less dependent on the grid resolution and the Reynolds number.

#### ACKNOWLEDGMENTS

The authors thank Professor Parviz Moin for his support and continued interest in this work. Y.M. was partially supported by a Grant-in-Aid from the Ministry of Education, Science, and Culture, Japan (No. 11750138), and also partially supported by the Center for Promotion of Computational Science and Engineering, Japan Atomic Energy Research Institute. O.V. was supported by the University of Missouri Research Board Grant.

<sup>1</sup>J. Smagorinsky, "General circulation experiments with the primitive equations. I. The basic experiment," *Mon. Weather Rev.* **91**, 99 (1963).

<sup>2</sup>M. Germano, U. Piomelli, P. Moin, and W. H. Cabot, "A dynamic subgrid-

scale eddy viscosity model," *Phys. Fluids A* **3**, 1760 (1991).

<sup>3</sup>Y. Morinishi and O. V. Vasilyev, "Subgrid scale modeling taking the numerical error into consideration," *CTR Annual Research Briefs—1998*, Stanford University/NASA Ames, 1999, p. 237.

<sup>4</sup>D. K. Lilly, "A proposed modification of the Germano subgrid scale closure method," *Phys. Fluids A* **4**, 633 (1992).

<sup>5</sup>B. Vreman, B. Geurts, and H. Kuerten, "Large-eddy simulation of the turbulent mixing layer," *J. Fluid Mech.* **339**, 357 (1997).

<sup>6</sup>S. Ghosal, "An analysis of numerical error in large-eddy simulation of turbulence," *J. Comput. Phys.* **125**, 187 (1996).

<sup>7</sup>Y. Morinishi, T. S. Lund, O. V. Vasilyev, and P. Moin, "Fully conservative higher order finite difference schemes for incompressible flow," *J. Comput. Phys.* **143**, 90 (1998).

<sup>8</sup>C. Meneveau and J. Katz, "Scale-invariance and turbulence models for large-eddy simulation," *Annu. Rev. Fluid Mech.* **32**, 1 (2000).

<sup>9</sup>Y. Morinishi and O. V. Vasilyev, "A recommended modification to the dynamic two-parameter mixed subgrid scale model for large eddy simulation of wall bounded turbulent flow," *Phys. Fluids* **13**, 3400 (2001).

<sup>10</sup>R. D. Moser, J. Kim, and N. N. Mansour, "Direct numerical simulation of turbulent channel flow up to  $Re_\tau=590$ ," *Phys. Fluids* **11**, 943 (1999).

<sup>11</sup>J. Bardina, J. H. Ferziger, and W. C. Reynolds, "Improved turbulence models based on large eddy simulation of homogeneous, incompressible, turbulent flows," Stanford University Tech. Rep. TF-19, 1983.

<sup>12</sup>Y. Zang, R. L. Street, and J. R. Koseff, "A dynamic subgrid-scale model and its application to turbulent recirculating flows," *Phys. Fluids A* **5**, 3186 (1993).

<sup>13</sup>B. Vreman, B. Geurts, and H. Kuerten, "On the formulation of the dynamic mixed subgrid-scale model," *Phys. Fluids* **6**, 4057 (1994).

<sup>14</sup>M. Salvetti and S. Banerjee, "A priori tests of a new dynamic subgrid-scale model for finite-difference large-eddy simulations," *Phys. Fluids* **7**, 2831 (1995).

<sup>15</sup>K. Horiuti, "A new dynamic two-parameter mixed model for large-eddy simulation," *Phys. Fluids* **9**, 3443 (1997).

<sup>16</sup>F. Sarghini, U. Piomelli, and E. Balaras, "Scale-similar models for large-eddy simulations," *Phys. Fluids* **11**, 1596 (1999).

<sup>17</sup>P. Sagaut, E. Garnier, and C. Seror, "Généralisation de l'identité de Germano et application à la modélisation sous-maille," *C. R. Acad. Sci., Ser. II: Mec., Phys., Chim., Sci. Terre Univers* **327**, 463 (1999).

<sup>18</sup>P. Sagaut, *Large Eddy Simulation for Incompressible Flows* (Springer-Verlag, Berlin, 2001), p. 116.